John von Neumann Institute for Computing

Spin-Polarized DFT Calculations and Magnetism

Rudolf Zeller

published in

Computational Nanoscience: Do It Yourself!,
J. Grotendorst, S. Blügel, D. Marx (Eds.),
John von Neumann Institute for Computing, Jülich,
NIC Series, Vol. **31**, ISBN 3-00-017350-1, pp. 419-445, 2006.

http://www.fz-juelich.de/nic-series/volume31

Spin-Polarized DFT Calculations and Magnetism

Rudolf Zeller

Institute of Solid State Research
Forschungszentrum Jülich
52425 Jülich, Germany
E-mail: ru.zeller@fz-juelich.de

The main aim of this presentation is to give an introduction into spin-polarized density-functional-theory (DFT) calculations as a method to predict and understand the band magnetism of itinerant electrons at zero temperature. It will be pointed out that, for instance the ferromagnetism of Fe, Co, and Ni is correctly predicted by such calculations without adjustable parameters and that the results can be explained in terms of a simple Stoner model. For practical applications it will be discussed why the convergence of density-functional self-consistency iterations can be very slow for magnetic systems and how this problem can be alleviated. As illustrating examples of recent applications in computational nanoscience, results for magnetic monatomic rows on noble metal substrates will be presented. Finally it will be argued that the magnetism in certain materials, for instance in antiferromagnets, does not arise from rigid-band shifts as in the Stoner model, but from covalent interactions between the electronic states of the participating atoms.

1 Introduction

Spin-polarized calculations within the framework of density-functional theory (DFT) are a powerful tool to describe the magnetism of itinerant electrons in solid state materials. Such calculations are not only the basis for a quantitative theoretical determination of spin magnetic moments, but can also be used to understand the basic mechanisms, which lead to the occurrence of magnetism in solid state materials. Since the original development of spin-density-functional theory by von Barth and Hedin[1] and Pant and Rajagopal[2] thousands of spin-polarized DFT calculations have been performed and published and it is thus entirely impossible to cover even the most relevant part of them. Therefore, the restricted aim of these lecture notes is the consideration of some aspects of zero-temperature spin magnetism in conceptually simple transition-metal solid state systems.

The tendency toward magnetism is determined by a competition between exchange and kinetic energy effects. Whereas the parallel alignment of the electronic spins leads to a gain of exchange energy, the alignment also causes a loss of kinetic energy. Contrary to the atoms, which usually are magnetic, most solid state systems are non-magnetic, since the gain in exchange energy is dominated by the loss in kinetic energy, which arises from the delocalization of the valence electrons in a solid. Only if these electrons are sufficiently localized, magnetism occurs as, for instance, in the elemental metals Fe, Co, Ni and Cr. These metals will serve here as examples to illustrate the predictive and explaining power of spin-polarized DFT calculations. The tendency toward magnetism is considerably enhanced in "lower-dimensional" systems like metallic surfaces and interfaces, multilayers, ultrathin films and wires, and magnetic clusters deposited on surfaces. These magnetic systems have received considerable experimental and theoretical attention in recent years and have been extensively studied by spin-polarized DFT calculations. Out of these calculation, I will consider here one typical "one-dimensional" example, the magnetism of

nanowires on metal substrates and present spin-density-functional results, which have been obtained by the Korringa-Kohn-Rostoker (KKR) method, which is introduced elsewhere in this Winter School on Computational Nanoscience.

The outline of my lecture notes is as follows. After an introduction to the underlying theory of spin-polarized density-functional calculations, it will be discussed how, in terms of the Stoner model, these calculations provide a basic description of the ferromagnetism of the elemental metals. This model will then be used to illustrate, why the self-consistency iterations for the solution of the density-functional equations in magnetic systems converge often rather slowly and how this can be avoided. Then follows a presentation of some recent results for magnetic monatomic wires. Finally, it is shown that the magnetism in certain solid state systems, in particular in the antiferromagnets, can be understood in terms of covalent interactions between the atoms, but not in terms of the Stoner model based on rigid band shifts.

2 Spin-Density-Functional Theory

If an external magnetic field is applied to an electronic system, it generally couples both to the electron spin and to the electronic orbital current. A framework for the description of spin coupling is provided by spin-density-functional theory, to which these lecture notes are restricted. For the description of orbital magnetism by density-functional approaches I refer to a recent Letter[3] and the references therein.

The basic variables of spin-density-functional theory are the scalar electronic density $n(\underline{r})$ and the vector of the magnetization density $\underline{m}(\underline{r})$. Instead of these four variables, alternatively the 2×2 spin density matrix $n^{\alpha\beta}(\underline{r})$ can be used, where the spin indices α and β can have two values, either $+$ for spin up (majority spin) or $-$ for spin down (minority spin). The notation $\uparrow$ instead of $+$ and $\downarrow$ instead of $-$ is also often used in the literature. The connection between $n(\underline{r})$, $\underline{m}(\underline{r})$ and $n^{\alpha\beta}(\underline{r})$ is given by

$$n(\underline{r}) = \sum_{\alpha} n^{\alpha\alpha}(\underline{r}) \qquad \underline{m}(\underline{r}) = \sum_{\alpha\beta} \underline{\sigma}^{\alpha\beta} n^{\alpha\beta}(\underline{r}) \tag{1}$$

and by

$$n^{\alpha\beta}(\underline{r}) = \frac{1}{2}\left(n(\underline{r})\delta^{\alpha\beta} + m_x(\underline{r})\sigma_x^{\alpha\beta} + m_y(\underline{r})\sigma_y^{\alpha\beta} + m_z(\underline{r})\sigma_z^{\alpha\beta}\right) \ . \tag{2}$$

Here 2×2 matrices are denoted by upper Greek indices and $\underline{\sigma} = (\sigma_x, \sigma_y, \sigma_z)$ is a vector consisting of the Pauli spin matrices

$$\sigma_x = \begin{pmatrix} 0 & 1 \\ 1 & 0 \end{pmatrix} \quad , \quad \sigma_y = \begin{pmatrix} 0 & -\mathrm{i} \\ \mathrm{i} & 0 \end{pmatrix} \quad , \quad \sigma_z = \begin{pmatrix} 1 & 0 \\ 0 & -1 \end{pmatrix} \ . \tag{3}$$

The Hohenberg-Kohn-Sham spin-density functional[1,2] is given by

$$\begin{aligned} E[n^{\alpha\beta}(\underline{r})] = T_s[n^{\alpha\beta}(\underline{r})] + \frac{e^2}{2}\int\int \frac{n(\underline{r})n(\underline{r'})}{|\underline{r} - \underline{r'}|}\mathrm{d}\underline{r}\mathrm{d}\underline{r'} \\ + \sum_{\alpha\beta}\int V_{ext}^{\alpha\beta}(\underline{r})n^{\alpha\beta}(\underline{r})\mathrm{d}\underline{r} + E_{xc}[n^{\alpha\beta}(\underline{r})] \end{aligned} \tag{4}$$

as a sum of the kinetic energy T_s of non-interacting electrons, the electron-electron interaction in the Hartree approximation, the interaction energy with the external potential $V_{ext}^{\alpha\beta}$ and the exchange-correlation energy. The external potential $V_{ext}^{\alpha\beta}$ contains the electrostatic Coulomb potential of the nuclei and perhaps the potential arising from a magnetic field. The minimum of the functional (Eq. (4)) is obtained by inserting the ground-state spin-density matrix and yields the ground-state energy. The variation of Eq. (4) with respect to $n^{\alpha\beta}(\underline{r})$ cannot be performed directly, since the explicit form of the density functional $T_s[n^{\alpha\beta}(\underline{r})]$ is not known. This problem can be solved with the help of single-particle wavefunctions (orbitals) $\varphi_i^\alpha(\underline{r})$, which allow to represent the kinetic energy functional $T_s[n^{\alpha\beta}(\underline{r})]$ and the spin-density matrix $n^{\alpha\beta}(\underline{r})$ as

$$T_s[n^{\alpha\beta}(\underline{r})] = \sum_{\alpha i} \int \varphi^{\star\,\alpha}_{\ i}(\underline{r}) \left(-\frac{\hbar^2}{2m} \nabla^2_{\underline{r}} \varphi_i^\alpha(\underline{r}) \right) \mathrm{d}\underline{r} \tag{5}$$

and as

$$n^{\alpha\beta}(\underline{r}) = \sum_i \varphi^{\star\,\alpha}_{\ i}(\underline{r}) \varphi_i^\beta(\underline{r}) \,, \tag{6}$$

where the sum over i includes all occupied orbitals. The last two equations provide an implicit representation of the kinetic energy in terms of the spin-density matrix and the minimum of Eq. (4) can now be found by variation of $E[n^{\alpha\beta}(\underline{r})]$ with respect to the single-particle wavefunctions. This leads to the Kohn-Sham equations

$$-\frac{\hbar^2}{2m} \nabla^2_{\underline{r}} \varphi_i^\alpha(\underline{r}) + \sum_\beta V_{eff}^{\alpha\beta}(\underline{r}) \varphi_i^\beta(\underline{r}) = \epsilon_i \varphi_i^\alpha(\underline{r}) \,, \tag{7}$$

where the ϵ_i represent Lagrange parameters, which guarantee that the wavefunctions are normalized as $\sum_\alpha (\varphi_i^\alpha, \varphi_i^\alpha) = 1$. The potential $V_{eff}^{\alpha\beta}$, which is defined as

$$V_{eff}^{\alpha\beta}(\underline{r}) = \delta^{\alpha\beta} e^2 \int \frac{n(\underline{r}')}{|\underline{r} - \underline{r}'|} \mathrm{d}\underline{r}' + V_{ext}^{\alpha\beta}(\underline{r}) + V_{xc}^{\alpha\beta}(\underline{r}) \,, \tag{8}$$

represents an effective one-particle potential. Useful approximations for the exchange-correlation energy functional can be given in terms of the eigenvalues $n^+(\underline{r})$ and $n^-(\underline{r})$ of the spin-density matrix $n^{\alpha\beta}(\underline{r})$. This matrix can be diagonalized as

$$\sum_{\alpha'\beta'} U^{\alpha\alpha'}(\underline{r}) n^{\alpha'\beta'}(\underline{r}) U^{\beta\beta'}(\underline{r}) = \delta^{\alpha\beta} n^\alpha(\underline{r}) \,, \tag{9}$$

where $U^{\alpha\beta}(\underline{r})$ are spin-1/2 rotation matrices and $n^\alpha(\underline{r})$ the eigenvalues. Note that these matrices and eigenvalues generally depend on the position $\underline{r}$. In many applications, for instance in ferromagnetic and antiferromagnetic solids, a common magnetization axis exists for all atoms. The z axis can then be chosen globally along the direction of the magnetic field and the spin-1/2 rotation matrices in Eq. (9) are independent of $\underline{r}$. This has the simplifying consequence that the energy and all other physical observables are functionals of the density and of the magnitude of the magnetization density $m(\underline{r}) = |\underline{m}(\underline{r})|$ rather than of the vector $\underline{m}(\underline{r})$. For a discussion of the more general situation of non-collinear magnetism, where the magnetization axis changes within the system, I refer to the presentation by Bihlmayer elsewhere in this Winter School on Computational Nanoscience.

In terms of the spin up and spin down orbitals $\varphi_i^+(\underline{r})$ and $\varphi_i^-(\underline{r})$, the spin densities $n^+(\underline{r})$ and $n^-(\underline{r})$ can be represented as

$$n^{\pm}(\underline{r}) = \sum_i |\varphi_i^{\pm}(\underline{r})|^2 \tag{10}$$

and the Kohn-Sham equations (7) for the orbitals can be written as

$$\left[-\frac{\hbar^2}{2m} \nabla_{\underline{r}}^2 + V_{eff}^{\pm}(\underline{r}) \right] \varphi_i^{\pm}(\underline{r}) = \epsilon_i^{\pm} \varphi_i^{\pm}(\underline{r}) \tag{11}$$

with the effective potential

$$V_{eff}^{\pm}(\underline{r}) = e^2 \int \frac{n(\underline{r'})}{|\underline{r} - \underline{r'}|} d\underline{r'} + V_{ext}^{\pm}(\underline{r}) + V_{xc}^{\pm}(\underline{r}) \; . \tag{12}$$

In an externally applied magnetic field H, the external potential $V_{ext}^{\pm}$ contains a field term $-(\pm \mu_B H)$, where the negative sign means that the majority (spin up: $+$) electrons are energetically favored compared to the minority (spin down: $-$) electrons. The exchange-correlation potential $V_{xc}^{\pm}(\underline{r})$, which is defined by the functional derivative of the exchange-correlation energy as

$$V_{xc}^{\pm}(\underline{r}) = \frac{\delta E_{xc}[n^+(\underline{r}), n^-(\underline{r})]}{\delta n^{\pm}(\underline{r})} \; , \tag{13}$$

can have different values for the two spin directions even without an external magnetic field. This is, for instance, realized in the ferromagnetic transition metals Fe, Co and Ni.

The spin-density-functional theory presented above is exact in principle, however the functionals E_{xc} and $V_{xc}^{\pm}$, in which all complications of the many-electron system are hidden, are not known and must be approximated. Useful approximation like the local-spin-density approximation[1,4,5] (LSDA), which depends locally on the spin densities, and the generalized gradient approximation (GGA)[6,7], which also depends on the gradients of the spin densities, have been developed and shown to be rather accurate for many applications.

3 Stoner Model for Ferromagnetism

It has independently been shown by several authors[8–11] that the spin-density formalism can be used to derive a Stoner model, which includes correlation effects, and to calculate the relevant Stoner parameter I. For this derivation it is convenient to switch from the spin densities $n^+(\underline{r})$ and $n^-(\underline{r})$ to the electron density

$$n(\underline{r}) = n^+(\underline{r}) + n^-(\underline{r}) \tag{14}$$

and the magnetization density

$$m(\underline{r}) = n^+(\underline{r}) - n^-(\underline{r}) \tag{15}$$

as variables to describe the system. Usually the magnetization $m(\underline{r})$ is a small parameter compared to the density $n(\underline{r})$. This means that the exchange-correlation potential can be expanded in terms of $m(\underline{r})$, which leads to the approximation

$$V_{xc}^{\pm}(\underline{r}) = V_{xc}^{o}(\underline{r}) \mp m(\underline{r}) \tilde{V}(n(\underline{r})) \; , \tag{16}$$

where the higher order terms in $m(\underline{r})$ are neglected and where $V^o_{xc}(\underline{r})$ is the exchange-correlation potential for non-spin-polarized electrons. The average value of $\tilde{V}(n(\underline{r}))$ is positive such that a more attractive potential acts on the majority electrons (with spin $+$) and a less attractive potential on the minority electrons (with spin $-$). Compared to Eq. (16) the Stoner model[12–14] uses the approximation

$$V^{\pm}_{xc}(\underline{r}) = V^o_{xc}(\underline{r}) \mp \frac{1}{2} IM \,, \tag{17}$$

where the potential difference is simulated by $\underline{r}$ independent constants. Here M is chosen as the local moment

$$M = \int_{\Omega} m(\underline{r}) \mathrm{d}\underline{r} \,, \tag{18}$$

which is given as an integral of the magnetization density $m(\underline{r})$ over the atomic unit cell Ω, and I is the exchange integral (= Stoner parameter). In ferromagnetic materials the moment M has the same value for all atoms. While the constant changes of the potential in (17) do not affect the wavefunctions $\varphi^{\pm}_i(\underline{r})$, which are identical to the non-magnetic ones, all eigenvalues $\epsilon^{\pm}_i$ are shifted by a constant amount $\mp\frac{1}{2}IM$. In periodic crystals the wavefunctions and eigenvalues are characterized by wavevectors $\underline{k}$ and band indices ν such that

$$\varphi^{\pm}_{\underline{k}\nu}(\underline{r}) = \varphi^o_{\underline{k}\nu}(\underline{r}) \qquad\qquad \epsilon^{\pm}_{\underline{k}\nu} = \epsilon^o_{\underline{k}\nu} \mp \frac{1}{2} IM \tag{19}$$

holds. The constant shift of the eigenvalues $\epsilon^{\pm}_{\underline{k}\nu}$ describes an exchange-splitting $\Delta = IM$ between the spin up and spin down bands and leads to the following representation

$$n^{\pm}(E) = \sum_{\nu} \int_{BZ} \delta(E - \epsilon^{\pm}_{\underline{k}\nu}) \mathrm{d}\underline{k} = n^o(E \pm \frac{1}{2} IM) \tag{20}$$

for the spin densities of states in terms of the density of states $n^o(E)$ of the non-magnetic system, where the integral in Eq. (20) is over the Brillouin zone (BZ). A good approximation of the constant shift $\pm\frac{1}{2}IM$ can be seen in in Figure 3, where realistic densities of states are shown, which were obtained by density-functional calculations in the local-spin-density approximation. From Eq. (20) one obtains the number N of electrons per atom and the moment M in the unit cell by integration over all occupied states below the Fermi energy E_F as

$$N = \int^{E_F} \left[n^o(E + \frac{1}{2} IM) + n^o(E - \frac{1}{2} IM) \right] \mathrm{d}E \tag{21}$$

and as

$$M = \int^{E_F} \left[n^o(E + \frac{1}{2} IM) - n^o(E - \frac{1}{2} IM) \right] \mathrm{d}E \,. \tag{22}$$

Since $n^o(E)$ is determined by the non-magnetic calculation and N by the condition of charge neutrality, the two equations (21) and (22) can be used to calculate the two unknown variables E_F and M. Equation (21) implicitly defines $E_F = E_F(M)$ as function of M. The moment M can then be determined by the equation

$$M = F(M) \,, \tag{23}$$

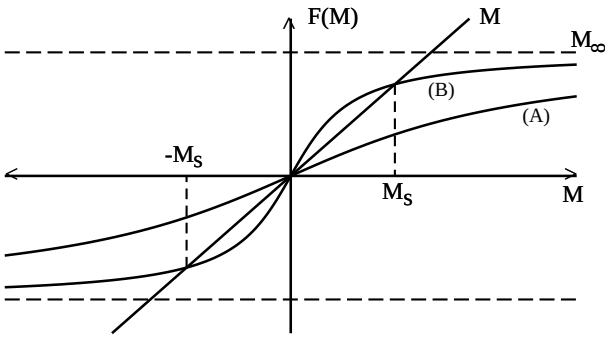

Figure 1. Graphical solution for the Stoner model. The intersection of $F(M)$ with the straight line M determines the solution M_s. The intersection at $M = 0$ is always a trivial solution.

where the function $F(M)$ is defined as

$$F(M) = \int^{E_F(M)} \left[n^o(E + \frac{1}{2}IM) - n^o(E - \frac{1}{2}IM) \right] \mathrm{d}E \,. \tag{24}$$

From the definition (Eq. (24)) one can easily derive that the function $F(M)$ satisfies the four conditions

$$F(M) = -F(-M) \,, \qquad F(0) = 0 \,,$$

$$F(\pm\infty) = \pm M_\infty \,, \qquad F'(M) > 0 \,,$$

where the last condition arises from the fact that the density $n^o(E)$ is always positive. Here M_∞ is the saturation magnetization for full spin-polarization, when all majority states are occupied and all minority states are empty. This situation corresponds to the atomic limit, where according to Hund's first rule the spin moment is maximal.

Two different possibilities for $F(M)$ are shown in Figure 1. For the function denoted by (A), the equation $M = F(M)$ has only the trivial non-magnetic solution $M = 0$. For the function denoted by (B) three solutions exist, $M = \pm M_S$ with a finite spontaneous magnetization and $M = 0$. This non-magnetic solution is however unstable. From Figure 1 it is clear that a solution with finite magnetization always exists, if the slope of $F(M)$ at $M = 0$ is larger than one. Thus $F'(0) > 1$ is a sufficient condition for ferromagnetic solutions. From Eq. (24) the derivative $F'(M)$ can be calculated as

$$\begin{aligned} F'(M) = \frac{I}{2} &\left[n^o(E_F + \frac{1}{2}IM) + n^o(E_F - \frac{1}{2}IM) \right] \\ &+ \left[n^o(E_F + \frac{1}{2}IM) - n^o(E_F - \frac{1}{2}IM) \right] \frac{\mathrm{d}E_F}{\mathrm{d}M} \,. \end{aligned} \tag{25}$$

For $M = 0$ the last equation simplifies to

$$F'(0) = In^o(E_F) \,, \tag{26}$$

and the sufficient condition for ferromagnetic solutions $F'(0) > 1$ can be written as

$$In^o(E_F) > 1 \,. \tag{27}$$

This is the famous Stoner criterion, which shows that a large exchange integral I and a large density of states $n^o(E_F)$ are properties, which are favorable for ferromagnetism.

The Stoner model can be extended to include the effects of an external magnetic field H. This allows to determine the spin susceptibility X, which according to $M = XH$ describes the behavior for small magnetic fields. Instead of Eq. (17) the relevant potential then is given by

$$V^{\pm}(\underline{r}) = V^o(\underline{r}) \mp \frac{1}{2} IM \mp \mu_B H \tag{28}$$

and instead of $M = F(M)$ the equation

$$M = F(M + \frac{2\mu_B H}{I}) \tag{29}$$

must be solved self-consistently. Linearizing (Eq. (29)) around M_0, which would be the magnetic moment without field, leads to

$$\begin{aligned} \Delta M = M - M_0 &= F(M + \frac{2\mu_B H}{I}) - F(M_0) \\ &\approx F'(M_0) \left(\Delta M + \frac{2\mu_B H}{I} \right) \\ &\approx \frac{1}{1 - F'(M_0)} F'(M_0) \frac{2\mu_B H}{I} \; . \end{aligned} \tag{30}$$

For $M_0 = 0$ the derivative $F'(M_0 = 0)$ is given by Eq. (26) and one obtains from Eq. (30) the result

$$M = \frac{1}{1 - In^o(E_F)} n^o(E_F) 2\mu_B H \; . \tag{31}$$

With $X = M/H$ the spin susceptibility is then given by

$$X = \frac{1}{1 - In^o(E_F)} n^o(E_F) 2\mu_B = SX^o \, , \tag{32}$$

where $X^o = n^o(E_F)2\mu_B$ is the Pauli spin susceptibility, which is obtained for non-interacting electrons if the exchange interaction is neglected. The exchange interaction leads to a Stoner enhancement factor $S = [1 - In^o(E_F)]^{-1}$, which diverges for $In^o(E_F) = 1$. The non-magnetic state is stable for $In^o(E_F) < 1$, whereas the ferromagnetic state is stable for $In^o(E_F) > 1$. Ferromagnetic behavior is therefore favored, if the exchange integral I is large, and even more important, if the density of states $n^o(E_F)$ at the Fermi energy E_F is large in the non-magnetic calculation.

The density of states usually shows a rather detailed structure. However, in a simple approximation one can assume that the density of states scales inversely to the bandwidth W. This inverse relation is exact for a constant density of states, since the integral of the density of states over the bandwidth

$$\int_W n_l^o \mathrm{d}E = 2l + 1 \tag{33}$$

is determined by the number of states for a given quantum number l, from which $n_l^o = (2l + 1)/W$ follows. For delocalized electrons the bandwidth is large and the density of states is small, whereas for more localized electrons the bandwidth is smaller and

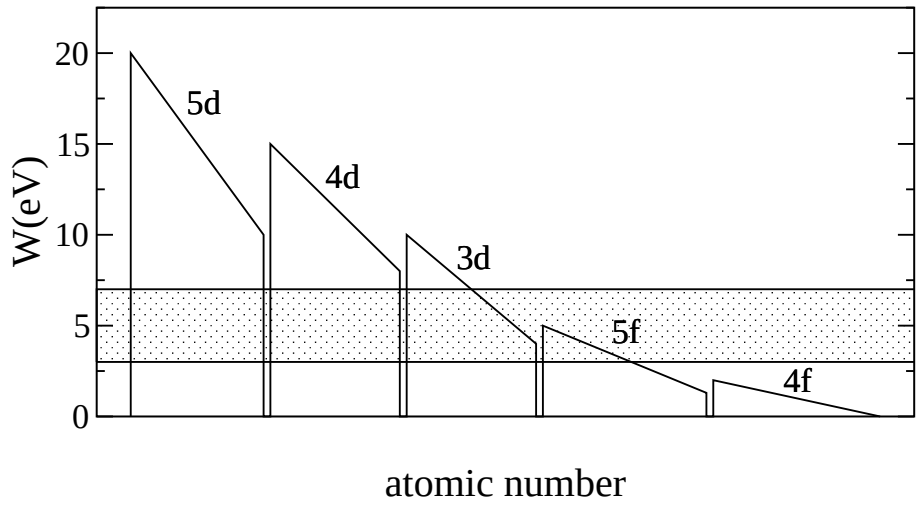

Figure 2. Schematic illustration for the bandwidth W of the transition metals ($3d$, $4d$ and $5d$ electrons), the rare earth metals ($4f$ electrons) and the actinides ($5f$ electrons). The shaded rectangle represents the region favorable for itinerant magnetism. Above the rectangle magnetism is suppressed and below the rectangle localized (atomic) magnetism is preferred.

the density of states larger. In the atomic limit the bandwidth goes to zero, the Stoner criterion is always satisfied and the magnetic moment attains its maximum according to Hund's first rule. Figure 2 shows a schematic representation for the bandwidths of the $3d$, $4d$ and $5d$ transition metals, the rare earth metals and the actinides. The $5f$ electrons of the early actinides and the $3d$ electrons of the late transition metals from Cr to Ni have a tendency for band magnetism, whereas the late actinides and the rare earth metals show localized magnetism with almost atomic moments in good agreement with Hund's rules.

The exchange integral I is an intra-atomic, element specific quantity, which in simplest approximation is independent of the local environment, which means independent of the structure and the site of a given atom, e.g., a surface, bulk or impurity atom. According to Gunnarsson[10] and Janak[15] the trend for the exchange integrals of the $3d$, $4d$ and $5d$ transition-metal series is

$$I_{3d} > I_{4d} > I_{5d}$$

which means that magnetism in the $3d$ elements is more likely than in the $4d$ and $5d$ elements. The same tendency for magnetism arises from the trend

$$n^o_{3d} > n^o_{4d} > n^o_{5d}$$

for the density of states, which corresponds to the bandwidth behavior

$$W_{3d} < W_{4d} < W_{5d}\ .$$

This behavior can be explained by the larger hybridization between d orbitals of larger quantum numbers because of their larger spatial extent as a consequence of the orthogonality condition, which these orbitals must satisfy with respect to the energetically lower lying orbitals of d and of s and p character.

metal	$n^o(E_F)[Ry^{-1}]$	$I[Ry]$	$In^o(E_F)$	$S = X/X_0$
Na	6.2	0.067	0.42	1.71
Al	5.6	0.045	0.25	1.34
Cr	9.5	0.028	0.27	1.36
Mn	21.	0.030	0.63	2.74
Fe	42.	0.034	1.43	-2.34
Co	27.	0.036	0.97	38.2
Ni	55.	0.037	2.04	-0.98
Cu	3.9	0.027	0.11	1.12
Pd	31.	0.025	0.78	4.46

Table 1. Densities of states $n^o(E_F)$ at the Fermi energy, exchange integral I, their product $In^o(E_F)$, and the Stoner enhancement factor S for some selected metals. These result have been obtained in density-functional calculations by the KKR method (from Ref. 15).

metal	$M_{LSDA}[\mu_B/atom]$	$M_{spin}[\mu_B/atom]$	$M[\mu_B/atom]$
Fe	2.15	2.12	2.22
Co	1.56	1.57	1.71
Ni	0.59	0.55	0.61

Table 2. Magnetic moments M_{LSDA} for Fe, Co and Ni calculated with the local-spin-density approximation in comparison with the experimental values for the spin-only moments M_{spin} and for the total moments M including the orbital contributions (from Ref. 17).

Quantitative results of non-spin-polarized density-functional calculations[15] in local-spin-density approximation for the density of states at E_F and for the exchange integral I are given in Table 1 for some selected metals. The results in Table 1 show that Fe and Ni satisfy the Stoner criterion $In^o(E_F) > 1$ and that Co with $In^o(E_F) = 0.97$ almost satisfies this criterion. It is discussed in Ref. 15 that the calculated values in Table 1 provide a lower bound to the susceptibility and that the Co value $In^o(E_F) = 0.97$ does not contradict the observed ferromagnetism for this metal. As a matter of fact in spin-polarized calculations[16,17], which do not use the Stoner model and do not rely on an estimate of I, the ferromagnetic state of Co has been found to be more stable than the non-magnetic state. Thus these early spin-density-functional calculations are consistent with the observed ferromagnetism of Fe, Co and Ni. The fcc metal Pd also has a large Stoner factor and is almost magnetic. The experimental Stoner factor for Pd is even approximately twice as large as the one given in Table 1 in agreement with the fact that the tendency for magnetism is underestimated by the approximation for I used in Ref. 15.

Figure 3 shows densities of states obtained by spin-density-functional calculations for bcc Fe and fcc Co. The densities of states have rather similar shapes for both spin directions and are only shifted with respect to each other by the exchange splitting $\Delta = IM$. Thus Eq. (20) is satisfied in good approximation and the Stoner model can be well applied for these metals. Fcc Ni has a similar density of states as Co, but with a smaller exchange splitting. The majority d states for Co and Ni are fully occupied, whereas in the minority states 1.7 electrons are missing for Co and 0.6 electrons for Ni. This leads to moments of

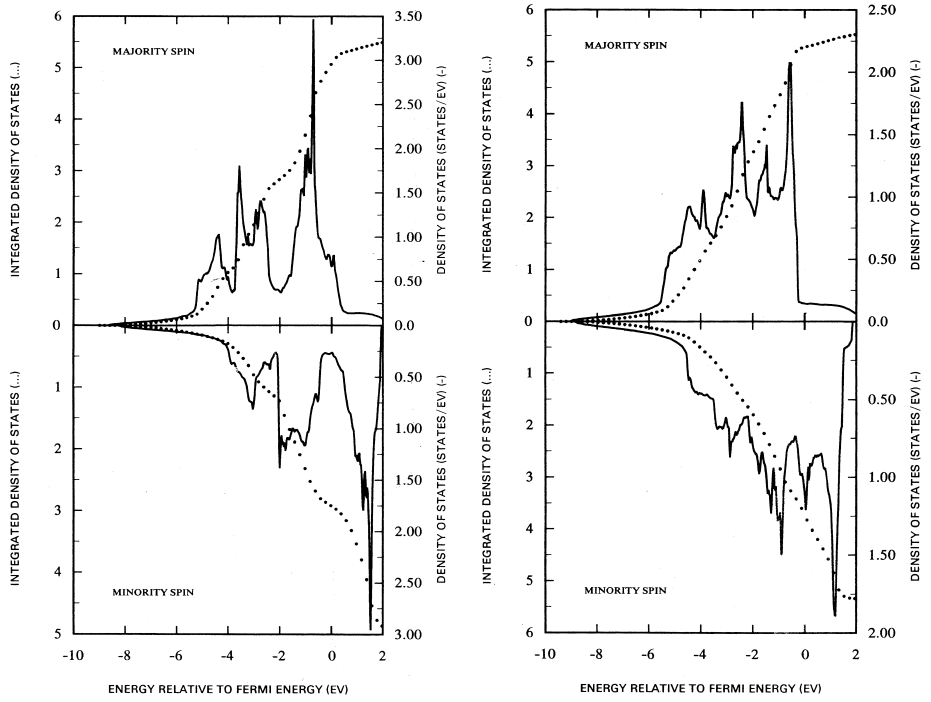

Figure 3. Density of states for bcc Fe (left picture) and fcc Co (right picture) from spin-density-functional calculations. The density of states for majority-spin electrons is plotted upwards and for minority-spin electrons downwards. States for negative energies (below E_F) are occupied, states for positive energies (above E_F) are unoccupied. The dotted curves represent the integrated density of states (from Ref. 17).

1.7 μ_B per Co atom and 0.6 μ_B per Ni atom. The moment for Fe is calculated as 2.2 μ_B. Table 2 shows that the calculated moments agree remarkably well with the experimental values, in view of the fact that the only input to these calculations are the atomic number and the crystal structures. Whereas the majority d states for Co and Ni are completely occupied, there are some empty majority d states in Fe. This difference has been historically characterized as *strong* magnetism for Co and Ni and *weak* magnetism for Fe, since empty d states make the magnetism less robust against environmental changes or, for instance, against pressure. However, it has been pointed out by Malozemoff *et al.*[18] that the pseudogap near the Fermi level in the minority d density of states for Fe also has a large stabilizing effect on the magnetism of Fe.

Figure 4 displays results of band structure calculations for fcc Co. The band structure is shown for high symmetry directions in the Brillouin zone. For each spin direction a separate band structure is obtained with a more or less constant band splitting. (In the Stoner model the splitting is independent of $\underline{k}$ according to Eq. (19).) The splitting in Figure 4 is only significant for the d bands. The parabolic s bands are barely split. Figure 4 shows that the majority d bands are completely below E_F in agreement with the fully occupied d density of states of Figure 3.

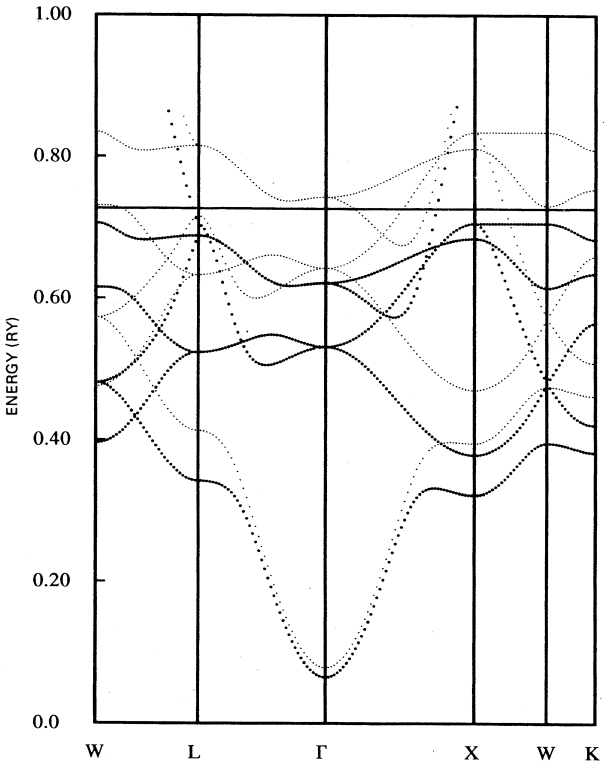

Figure 4. Band structure for fcc Co from spin-density-functional calculations. Bands for majority electrons are indicated by large points and for minority electrons by small points (from Ref. 17).

4 Self-Consistency Iterations

The density-functional equations (6-8) or (10-12) must be solved self-consistently, since the density is given in terms of the orbitals, which depend on the effective potential, which again depends on the density. The resulting nonlinear self-consistency problem, which may be written in the form

$$n(\underline{r}) = F_{\underline{r}}[n] \tag{37}$$

can only be solved by iteration

$$n_{i+1}(\underline{r}) = F_{\underline{r}}[n_i] \tag{38}$$

since other methods are not available. Very often, however, this standard iteration process diverges and leads to density oscillations of increasing amplitude. Then the iteration process must be modified to damp these oscillations. A damping is obtained if the iteration (Eq. (38)) is replaced by a modified iteration

$$n_{i+1} = \alpha F_{\underline{r}}[n_i] + (1-\alpha) n_i \tag{39}$$

with a suitably chosen mixing parameter α. It has been shown[19] that the convergence behavior of (38) is determined by the eigenvalues λ of a matrix $f(\underline{r},\underline{r'})$, which is defined as the functional derivative of $F_{\underline{r}}[n]$ with respect to $n(\underline{r'})$. It has also been shown[19] that these eigenvalues are real and that they must satisfy $\lambda < 1$, where this inequality arises from the stability condition for the solution of $n = F_{\underline{r}}[n]$.

The convergence of the iteration process (Eq. (38)) requires that the eigenvalues λ are in the range $-1 < \lambda < 1$, which is, however, often not satisfied, since large negative eigenvalues can exist. On the other hand, the iteration process (Eq. (39)) requires that the eigenvalues λ are in the range defined by

$$-1 < \alpha\lambda + 1 - \alpha < 1\,. \tag{40}$$

This condition can always be satisfied if $\alpha > 0$ is chosen small enough. By rewriting $\alpha\lambda + 1 - \alpha < 1$ as $\alpha\lambda < \alpha$, it is clear that the right inequality in Eq. (40) is satisfied for positive α because of the stability condition $\lambda < 1$. By rewriting $-1 < \alpha\lambda + 1 - \alpha$ as $\alpha(1-\lambda) < 2$ or due to $1 - \lambda > 0$ as

$$\alpha < \frac{2}{1-\lambda}\,, \tag{41}$$

where the right-hand side is positive because of $\lambda < 1$, it is clear that the left inequality in Eq. (40) can be satisfied if α is chosen small enough. Thus the largest α, for which the iteration process still converges, is determined by the negative eigenvalue λ with the largest absolute value. Unfortunately, this value can be rather large leading to rather small α's, in particular if charge transfer occurs between the atoms in the considered system. Also intra-atomic charge transfers, for instance between the $4f$ and $5d$ shells of rare-earth metals, can lead to rather small values of suitable α's. The main disadvantage of small values for α is that only a small amount of the output density $F_{\underline{r}}[n_i]$ is mixed with the input density n_i in Eq. (39). Thus the iterations only slowly move away from the first guess n_0 for input density and many iterations are required to find the self-consistent solution. It is well known that more sophisticated mixing schemes can be used to speed the iterations, for instance the Anderson[20] and Broyden[21] mixing schemes. A comprehensive discussion of these schemes can be found in Refs. 22 and 23.

The slow convergence of the density iterations (Eq. (39)) due to a small mixing parameter α is a particular problem in spin-density functional calculations, if the system is near the threshold between a magnetic or non-magnetic state. This can be illustrated by the Stoner model. Figure 5 shows the iteration process $M_{i+1} = F(M_i)$ for the solution of $M = F(M)$ for two possible situations, if a magnetic solution exists (upper picture) and if the system is almost magnetic with $F'(0) \approx 1$ (lower picture). The iterations $M_{i+1} = F(M_i)$ always converge, since $F'(M_s) < 1$ is valid at the solution M_s, but near the threshold many iterations are necessary to approach the solution $M_s = 0$. If now, as required by the density iterations (Eq. (39)), the iteration process is modified into the much slower iteration process $M_{i+1} = \alpha F(M_i) + (1-\alpha)M_i$, the convergence is extremely slow and an enormous number of iterations is required.

This problem can be solved to some extent by the observation[19] that near $M_s = 0$ the convergence of the density and the convergence of the magnetization are practically decoupled because of $m(\underline{r}) \ll n(\underline{r})$. This decoupling allows to introduce two different

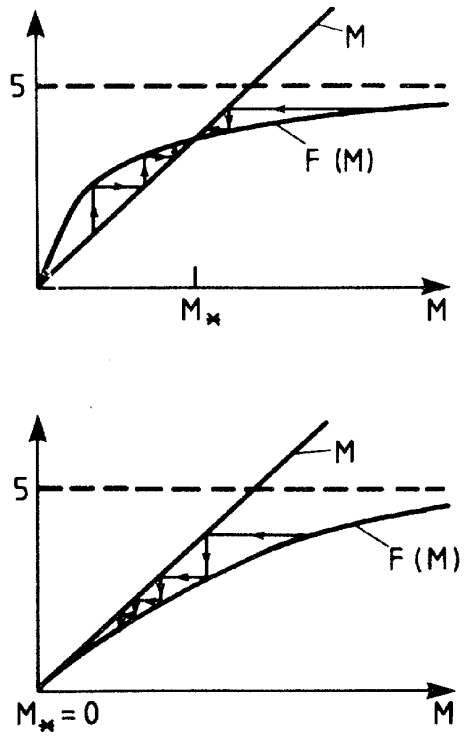

Figure 5. Schematic representation of the iteration process $M_{i+1} = F(M_i)$ for a magnetic system (above) and a non-magnetic system (below). Both iteration processes converge, since $F'(M) < 1$. The convergence is illustrated by the straight lines, where the arrows indicate the direction of the iteration process. Lines with vertical arrows represent the mapping from M to $F(M)$ and horizontal lines the choice of $F(M)$ as the input M for the next iteration (from Ref. 19).

mixing parameters α_n and α_m for the density and the magnetization

$$\begin{aligned} n_{i+1} &= \alpha_n F_{\underline{r}}[n_i, M_i] + (1-\alpha_n) n_i \\ m_{i+1} &= \alpha_m F_{\underline{r}}[n_i, M_i] + (1-\alpha_m) n_i \,, \end{aligned} \tag{42}$$

where α_m can be chosen much larger than α_n, which considerably improves the convergence near the threshold $F'(0) = 1$. It should be noted that for the Anderson and Broyden mixing schemes a choice of different mixing parameters is not useful, since these schemes are based on a simultaneous minimization of the errors of the density and the magnetization in a multidimensional space and this minimization automatically adapts to the different iteration behavior of the density and the magnetization. On the other hand, contrary to Eq. (39) which converges to a stable solution, the Anderson and Broyden mixing schemes can also converge to unstable solutions. This means that these schemes can easily miss a magnetic solution near the threshold $F'(0) \approx 1$ by improperly converging to the unstable non-magnetic solution.

5 Nanowires

Whereas atoms are usually magnetic, the occurrence of magnetism in the elemental solids is rather an exception. For instance, none of the sp bonded elements and only five of 30 d bonded transition metals are magnetic in their bulk crystalline phase: Co and Ni are ferromagnetic, Cr is antiferromagnetic, and Mn and Fe are ferromagnetic or antiferromagnetic depending on their crystal structure. The main reason preventing magnetism is the overcompensation of the gain in exchange energy by a loss in kinetic energy which occurs for small values of the density of states $n^o(E_F)$ at the Fermi level. Since the exchange integral I is more or less independent of the local environment of a atom in the solid, magnetism in alloys, at surfaces, for impurities in bulk systems and for adatoms at surfaces occurs mainly because of larger values of $n^o(E_F)$ arising from smaller bandwidths. The reduced bandwidth in these system is a consequence of reduced atomic coordination numbers, which leads to less hybridization between the electrons. This can be explained by simple nearest-neighbor tight-binding models, where the bandwidth scales like $W \sim \sqrt{N_c}$. For instance, the coordination number N_c of an atom in a fcc crystal is $N_c = 12$, for an atom in the (100) surface of a fcc crystal it is $N_c = 8$, and at the $(100) \times (111)$ and $(100) \times (110)$ step edges at terraces on the fcc (100) surface (see Figure 6), the coordination numbers are $N_c = 7$ and $N_c = 6$.

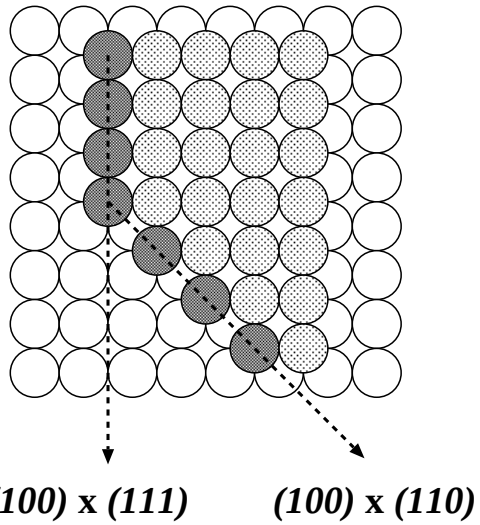

Figure 6. Step edges at the fcc (100) terrace. The step notation from Ref. 24 is used.

From these coordination numbers one expects the bandwidths scale like

$$W_{(100)\times(110)} : W_{(100)\times(111)} : W_{(100)} : W_{fcc} = 0.71 : 0.76 : 0.82 : 1.00$$

and that the densities of states scale like

$$n_{(100)\times(110)} : n_{(100)\times(111)} : n_{(100)} : n_{fcc} = 1.41 : 1.31 : 1.22 : 1.00\ .$$

Thus the tendency toward magnetism should be larger at surfaces than in bulk crystals, larger for atoms in step edges than for atoms embedded in flat surfaces and larger for adatoms on surfaces than for the atoms in step edges. Even smaller coordination numbers appear in free-standing monolayers and monowires and an even larger tendency toward magnetism can be expected for these systems. Of course, the experimental realization of such free-standing systems seems to be difficult, but when such layers or wires are supported on non-magnetic substrates, the tendency toward magnetism can still be rather high, if the hybridization with substrate electronic states is small. Examples for such systems are transition-metal layers and wires on noble metal substrates. For a discussion of magnetic properties of thin layers I refer to recent reviews[25–27] and the references therein. Spin-polarized DFT calculations for magnetic nanowires have been performed by Weinert and Freeman[28] already in 1983 and by many groups in the last few years[29–50], where this list of references is certainly not complete. Since a discussion of these studies is beyond the scope of the present lecture, I will present here only some of our own results[33] for $4d$ monatomic wires on the Ag surface. These results have been obtained by the screened Korringa-Kohn-Rostoker (KKR) method[51–54], which is well suited for such calculations because of its linear $O(N)$ scaling as discussed elsewhere in this Winter School on Computational Nanoscience.

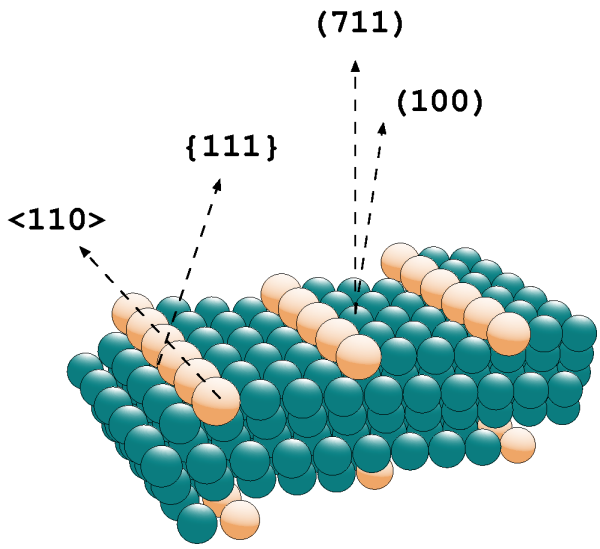

Figure 7. The fcc (711) vicinal surface with decorated steps as an example of periodically repeated monatomic wires, here at the $(100) \times (111)$ step edge (from Ref. 33).

In our calculations we have exploited the concept of step decoration on vicinal surfaces. These are surfaces with high Miller indices, for instance the fcc (711) surface shown in Figure 7. The same concept of step decoration is also exploited in the experimental preparation of extended ultrathin nanowires, where the arrays of parallel steps on these vicinal surfaces are used as templates along which the deposited material can nucleate. The darker

spheres in Figure 7 represent the Ag atoms and the lighter spheres the monatomic rows of $4d$ transition-metal atoms. The same geometry can also be used to describe monatomic rows on the middle of the terraces, if some rows of Ag atoms on the right-hand side of the transition-metal row are removed.

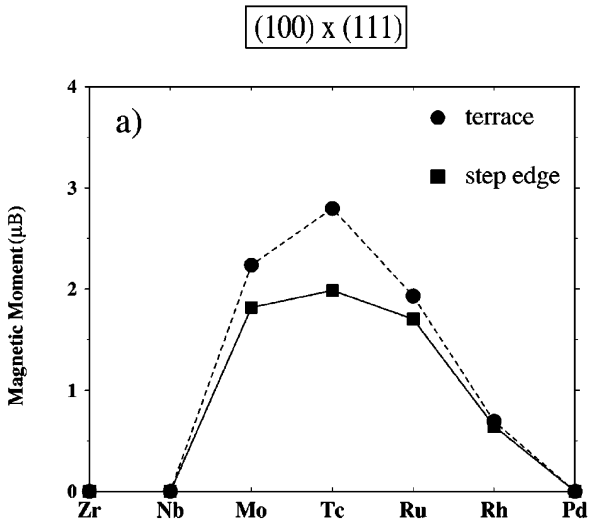

Figure 8. Magnetic moments of $4d$ monatomic rows on the fcc Ag(711) vicinal surface. Results denoted by circles are for rows in terrace and results denoted by squares for rows in step edge positions (from Ref. 33).

The calculated magnetic moments per atom for $4d$ magnetic monatomic wires on fcc (711) and fcc (410) Ag vicinal surfaces are shown in Figs. 8 and 9. A direct comparison between the magnetic moments for the two different step orientations shows that the magnetic moments for $(100) \times (111)$ wires are smaller than for the $(100) \times (110)$ wires for all elements except for Rh. The main reason for this difference is the increased hybridization of the $4d$ states between the atoms in the more closely packed $(100) \times (111)$ wires (see Figure 6), which leads to larger bandwidths and smaller densities of states $n^o(E_F)$. For Rh the situation is different. Whereas in non-magnetic calculations the local density of states for the Nb, Mo, Tc, and Ru wires shows a peak near the Fermi level, which due to broadening is reduced in height leading to a lower value of $n^o(E_F)$ in the close-packed rows, the non-magnetic density of states for the Rh wires has a peak below the Fermi level such that broadening leads to an increase of $n^o(E_F)$. Pictures for these non-magnetic densities of states can be found in Ref. 33.

Another feature evident in Figs. 8 and 9 is that the rows at the step edges (solid lines) have smaller moments than the rows on the terraces (dashed lines). This can be explained by an increase in the hybridization between the extended $4d$ orbitals of the row atoms and the sp like valence electrons of the substrate Ag atoms. Since the extent of the $4d$ orbitals is larger at the beginning of the $4d$ series, this effect is more pronounced at the beginning of the $4d$ series. The importance of the hybridization with the Ag substrate has also been

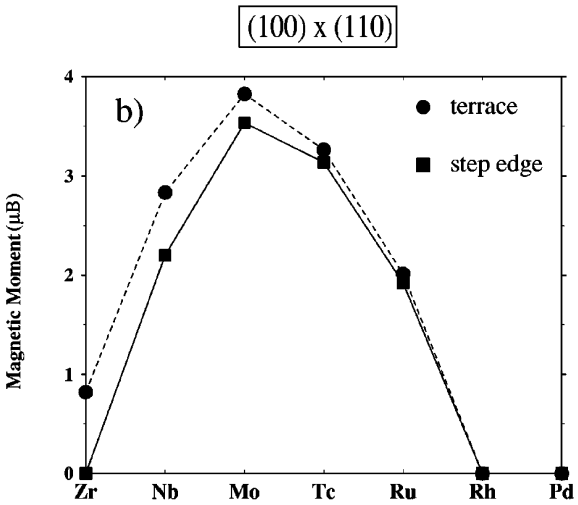

Figure 9. Magnetic moments of $4d$ monatomic rows on the fcc Ag(410) vicinal surface. Results denoted by circles are for rows in terrace and results denoted by squares for rows in step edge positions (from Ref. 33).

observed in spin-polarized DFT calculations for $4d$ dimers[55], where the magnetism of free dimers from the beginning of the $4d$ series (Y, Zr, Nb) is completely quenched, if they are adsorbed on the Ag(100) surface.

In addition to the ferromagnetic solutions shown in Figs. 8 and 9, we have also found antiferromagnetic solutions for Nb, Mo, and Tc wires, where the atoms in the rows have moments of alternating sign. In general, our results are in good agreement to similar calculation by Spisak and Hafner[39], who have used a quite different computational approach, the Vienna *ab initio* simulation package[56, 57] (VASP) in a projector augmented-wave (PAW) representation. Both methods, KKR and VASP, have shown that antiferromagnetism is preferred for Nb and Mo wires, that the ferromagnetic and antiferromagnetic states for Tc wires are almost degenerated in energy and that ferromagnetism is preferred in Ru and Rh wires. Compared to the KKR calculations, the VASP calculations have found somewhat larger moments and larger magnetic energy differences. In addition, the VASP calculations have found a metastable ferromagnetic solution for Nb wires and a metastable antiferromagnetic solution for Ru wires. These differences are probably related to the inclusion of gradient corrections to the exchange-correlation potential in Ref. 39 and to the spherical potential approximation used in Ref. 33.

6 Beyond the Stoner Model

The explanation of spin magnetism in terms of the Stoner model as discussed above is restricted to ferromagnetic materials, where all atoms have identical moments as in the elemental ferromagnets, and to ferromagnetic systems like magnetic overlayers, wires and impurities in contact to non-magnetic system, if the magnetic polarization of the non-magnetic atoms is small and its contribution can be neglected. For instance, it has been

shown[58] that a Stoner criterion $In^{o}_{loc}(E_F) > 1$ very similar to Eq. (27) can be used to characterize the behavior of magnetic impurities in non-magnetic materials. Here $n^{o}_{loc}(E)$ is the local density of states obtained by integrating the electron distribution over the impurity cell and neglecting contributions from the non-magnetic host atoms. The exchange integrals (Stoner parameters) for impurities are rather similar to the ones given in Table 1. This discussion for impurities is easily generalized for magnetic monolayers[59] and monowires[33], which are supported on non-magnetic substrates or free-standing in vacuum.

However, in magnetic systems, which consist of atoms with different moments, like magnetic alloys, antiferromagnets, magnetic monolayers and monowires on magnetic or almost magnetic substrates, or magnetic impurities in magnetic or almost magnetic hosts, the discussion within the Stoner model can fail. The failure arises in systems, where the main assumption of Stoner model, which is the rigid-band shift of the spin-dependent densities of states, is not satisfied. In these systems the magnetism cannot be explained by the Stoner model, but alternatively by spin-dependent changes in the covalent interaction[60] between the electronic states of neighboring atoms.

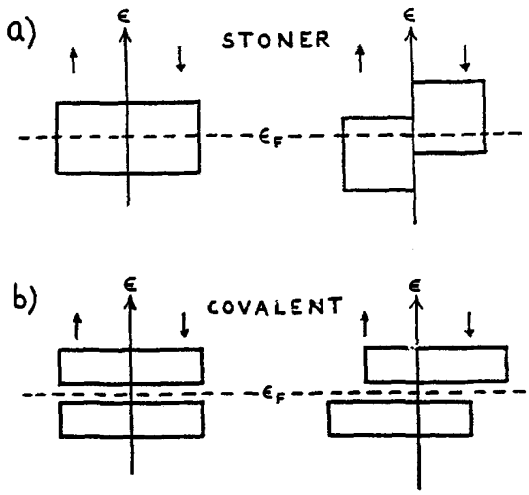

Figure 10. Schematic changes in the majority (↑) and minority (↓) spin densities of states, which lead to magnetism (from Ref. 60).

The distinction between "Stoner" or "covalent" magnetism is illustrated in Figure 10. On the left the densities of states are given for the non-magnetic and on the right for the magnetic situation. Whereas in the Stoner model the densities of states are shifted and magnetism occurs because a high density of states at the Fermi level makes the non-magnetic state unstable, for covalent magnetism the density of states at the Fermi level does not play a special role and magnetism is connected with a spectral-weight shift of the densities of states. The physical mechanism for the spectral-weight shift can be seen in its simplest from in the states of a diatomic molecule as illustrated in Figure 11.

When the states of the individual atoms interact, bonding and anti-bonding hybrids are formed. When the interacting states are degenerated ($\epsilon_1 = \epsilon_2$), the spectral weight is

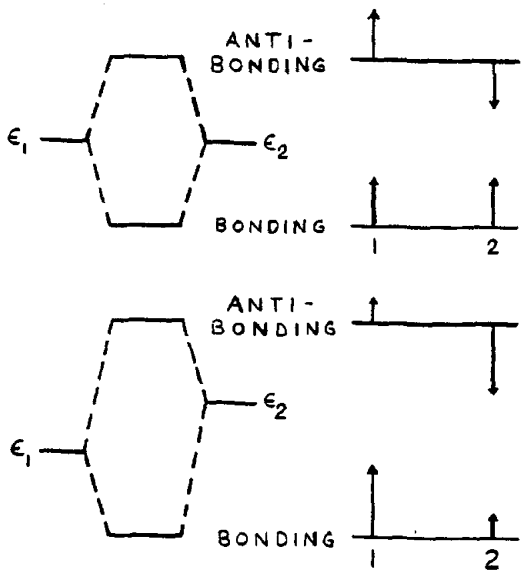

Figure 11. Changes in energy levels (left) and wavefunction weights (right) of covalent bonds caused by a relative displacement of the individual atomic levels ϵ_1 and ϵ_2 (from Ref. 60).

evenly distributed in both hybrids (upper right-hand portion of Figure 11). When one of the interacting states is displaced relative to the other ($\epsilon_1 < \epsilon_2$), for instance as a consequence of a larger moment on atom 1, the spectral weight is shifted within each hybrid (lower right-hand portion of Figure 11). The bonding hybrid obtains more weight on atom 1 with the lower energy level ϵ_1 and the anti-bonding hybrid obtains more weight on atom 2 with the higher energy level ϵ_2. This spectral-weight shift leads to a charge transfer and is responsible for the covalent magnetism. Note that Figure 11 refers to the interaction of states of only one spin direction, for the other spin direction a similar picture applies with $\epsilon_1 > \epsilon_2$. The combined effect of both hybridizations leads to the densities of states shown in the lower right-hand portion of Figure 10.

The different hybridization behavior between ferromagnetically and antiferromagnetically aligned atoms has also been explained in detail for spin-polarized DFT calculations for interacting impurity pairs in Cu and Ag[61]. In antiferromagnetic systems the special situation occurs that, although the atoms are chemically equivalent with the same exchange integral I, they are magnetically different with alternating moments M and $-M$. The essential quantity, which decides upon the stability of the antiferromagnetic state, is again the spin-dependent susceptibility, which in first order perturbation theory connects the moment with the magnetic field

$$M = X_{AF} H \,, \tag{45}$$

where AF denotes antiferromagnetism and where the fictive field is assumed to point into the same direction as the moments thus representing an alternating staggered field. The

magnetic field and the magnetic moments lead to potentials

$$V_1^{\pm} = V^o + \Delta V_1^{\pm} = V^o \pm \left(\frac{1}{2} IM + \mu_B H\right) \tag{46}$$

and

$$V_2^{\pm} = V^o + \Delta V_2^{\pm} = V^o \mp \left(\frac{1}{2} IM + \mu_B H\right) , \tag{47}$$

where $V_1^{\pm}$ stands for the potentials on the atoms in the sublattice with odd indices and $V_2^{\pm}$ for the potentials on the atoms in the sublattice even indices. The self-consistency conditions for the moment of atom $i = 0$ is given by

$$M = \int^{E_F(M)} [n_0^+(E) - n_0^-(E)] \mathrm{d}E \tag{48}$$

as above in Eq. (22), but with the difference that $n_0^{\pm}(E)$ cannot be obtained by a simple shift from the non-magnetic density of states. By using basic properties of the Green function of the one-particle Schrödinger equation, which are given in the appendix, the moment M in (48) can be calculated as

$$\begin{aligned} M &= -\frac{1}{\pi} \mathrm{Im} \int^{E_F(M)} [G_{00}^+(E) - G_{00}^-(E)] \mathrm{d}E \\ &= -\frac{1}{\pi} \sum_i \mathrm{Im} \int^{E_F(M)} G_{0i}^o(E) \left[\Delta V_i^+ - \Delta V_i^-\right] G_{i0}^o(E) \mathrm{d}E + O(\Delta V_i^3) . \end{aligned} \tag{49}$$

Linear in ΔV the last equation can be written as

$$M = X_{AF}^o \left(\frac{IM}{2\mu_B} + H\right) , \tag{50}$$

where $\Delta V_i^{\pm}$ from Eqs. (46) and (47) was used and where the susceptibility X_{AF}^o for non-interacting electrons is defined as

$$X_{AF}^o = \frac{2\mu_B}{\pi} \mathrm{Im} \int^{E_F(M)} \left[\sum_{\mathrm{even}\, i} G_{0i}^o(E) G_{i0}^o(E) - \sum_{\mathrm{odd}\, i} G_{0i}^o(E) G_{i0}^o(E)\right] \mathrm{d}E . \tag{51}$$

This susceptibility can also be written as

$$X_{AF}^o = \frac{2\mu_B}{\pi} \mathrm{Im} \int^{E_F(M)} \left[\sum_{\mathrm{all}\, i} G_{0i}^o(E) G_{i0}^o(E) - 2 \sum_{\mathrm{odd}\, i} G_{0i}^o(E) G_{i0}^o(E)\right] \mathrm{d}E . \tag{52}$$

Here by use of Eqs. (64) and (62) the first term can be expressed by the density of states $n^o(E_F)$ and X_{AF}^o can be written as

$$X_{AF}^o = 2\mu_B \left[a(E_F) - n^o(E_F)\right] , \tag{53}$$

where the function $a(E_F)$ is defined second term in Eq. (52). If Eq. (50) is solved for M, one obtains

$$M = X_{AF} H = \left(1 - \frac{I X_{AF}^o}{2\mu_B}\right)^{-1} X_{AF}^o H = S_{AF} X_{AF}^o H , \tag{54}$$

which shows that the spin susceptibility X_{AF}, similarly as in ferromagnets, is enlarged compared to X^o_{AF} by an enhancement factor S_{AF}. The criterion for a stable antiferromagnetic state is

$$\frac{IX^o_{AF}}{2\mu_B} > 1\,. \tag{55}$$

By using Eq. (53) the criterion can be written as

$$I\left[a(E_F) - n^o(E_F)\right] > 1 \tag{56}$$

which shows that a high density of states $n^o(E_F)$ at the Fermi energy is unfavorable for antiferromagnetism.

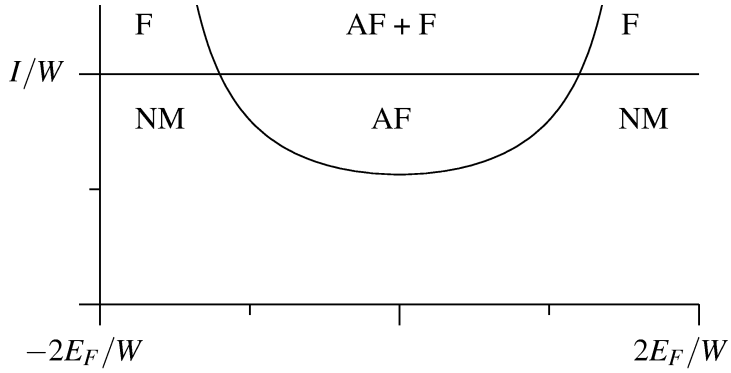

Figure 12. Phase diagram for a model with a rectangular density of states. The stability region for the nonmagnetic state is indicated by NM, the stability regions for the ferromagnetic or antiferromagnetic state are indicated by F or AF.

For a simple model with a rectangular density of states $n^o(E) = 1/W$ for $-W/2 < E < W/2$ and $n^o(E) = 0$ for $|E| > W/2$, it is possible to determine $a(E_F)$ approximately from the imaginary and real part of the Green function $G^o(E)$ and to derive the phase diagram shown in Figure 12. The imaginary part of the Green function for this model is given by $\mathrm{Im}G^o_{00}(E) = -\pi/W$ for $-W/2 < E < W/2$ and vanishes for $|E| > W/2$. The real part follows from the Kramers-Kronig relation (Eq. (62)) as

$$\mathrm{Re}G^o_{00}(E) = -\frac{1}{W}\ln\left|\frac{E - W/2}{E + W/2}\right|\,. \tag{57}$$

To evaluate $a(E_F)$ approximately, the main contribution arising from atom $i = 0$ is taken into account and the contributions $G^o_{0i}(E)G^o_{i0}(E)$ of all other atoms $i \neq 0$ are neglected, since they decay with increasing distance between the atoms i and 0. From $\mathrm{Im}(G^o_{00})^2 = 2\mathrm{Re}G^o_{00}\mathrm{Im}G^o_{00}$ the result

$$a(E_F) - n^o_0(E_F) = \frac{1}{W}\left[\frac{4}{W}\int_{-W/2}^{E_F}\ln\left|\frac{E - W/2}{E + W/2}\right|\mathrm{d}E - 1\right] \tag{58}$$

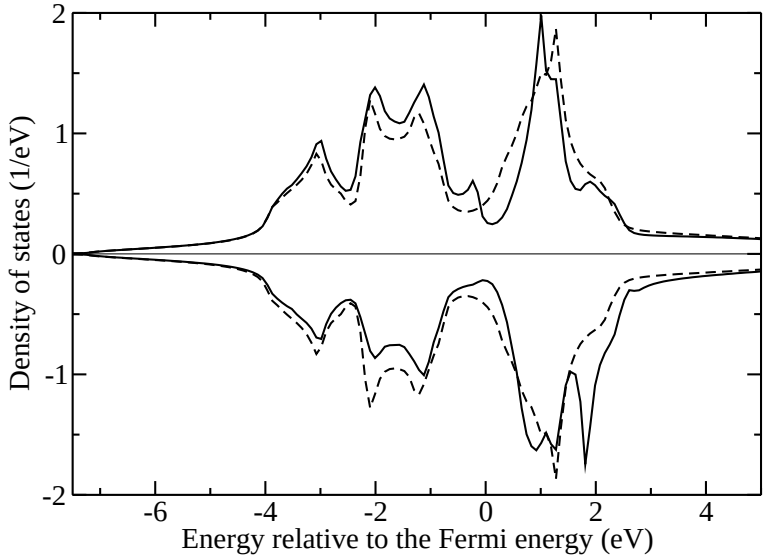

Figure 13. Density of states for one atom in antiferromagnetic bcc Cr (solid curves) compared to the density of states for one atom in nonmagnetic bcc Cr (dashed lines) The density of states for majority-spin electrons is plotted upwards and for minority-spin electrons downwards. The density of states for the other atom are obtained by interchanging spin up and spin down curves.

follows for $|E_F| < W/2$. The stability criterion (Eq. (56)) can be written as $I > [a(E_F) - n_0^o(E_F)]^{-1}$ or as

$$\frac{I}{W} > \left[2 \int_{-1}^{2E_F/W} \ln \left| \frac{x-1}{x+1} \right| \mathrm{d}x - 1 \right]^{-1} , \tag{59}$$

which is obtained from Eq. (58) by the substitution $x = 2E/W$. The right-hand side of Eq. (59) defines a function $f(2E_F/W)$, which is shown as the bended curve in Figure 12. Above this curve the antiferromagnetic state is more stable and above the straight line at I/W the ferromagnetic state is more stable than the non-magnetic state. For $E_F = 0$ at center of the band, the function $f(2E_F/W)$ attains its minimum with the value $[4 \ln 2 - 1]^{-1} = 0.564... < 1$. This shows that a position of the Fermi energy E_F near to the band center makes antiferromagnetism more favorable than ferromagnetism.

For the $3d$ metal Cr, the Fermi energy is in the middle of the d band and furthermore lies in a pseudogap with a reduced $n^o(E_F)$ such that antiferromagnetism should be even more preferred for Cr than for the model with the phase diagram of Figure 12. To illustrate the situation for Cr, I have performed self-consistent density-functional calculations in the local-spin-density approximation[4] by the full-potential KKR method as described in Ref. 62 using $l_{max} = 3$ for t matrices and Green functions and $l_{max} = 6$ for the density and the potential. To calculate the densities of states shown in Figure 13, I have used a lattice constant of 0.294 nm, which is two percent larger than the experimental value 0.288 nm. This leads to a moment of 1.08 μ_B and increases the differences shown in Figure 13 compared to calculations for the experimental lattice constant with a moment of 0.39 μ_B.

The calculated density of states clearly shows the spectral-weight shift for the occupied states. Thus Figure 13 illustrates that the mechanism of covalent interaction discussed above (compare Figure 10) explains the antiferromagnetism in Cr.

Note, however, that the real ground-state of Cr is not the antiferromagnetic state, but an incommensurate spin-density wave state. The consideration of this state is beyond the scope of my presentation and I refer to Refs. 63 and 64 for a discussion about the applicability of spin-polarized DFT calculations for the incommensurate spin-density wave state of Cr.

Appendix

Green-Function Properties

The Green function $G(E)$ for a Hamilton operator $\mathcal{H}$ is defined by the operator equation

$$G = \frac{1}{E - \mathcal{H}} \,, \tag{60}$$

where the energy E is chosen as a complex quantity. For real energies it is necessary to perform a limiting process. Then the real energy E is replaced by $E + i\epsilon$ and all equations are understood in the sense that the limit $\epsilon \to 0+$ must be performed in the end. The relation

$$\lim_{\epsilon \to 0+} \frac{1}{E + i\epsilon - \mathcal{H}} = P\frac{1}{E - \mathcal{H}} - i\pi\delta(E - \mathcal{H}) \,, \tag{61}$$

where P denotes the principal value, establishes the connection between the imaginary part of the Green function and the density of states $n(E) = \delta(E - \mathcal{H})$ and also the Kramers-Kronig relation between the imaginary and the real part of the Green function

$$\mathrm{Im}G(E) = -\pi n(E) \,, \qquad \mathrm{Re}G(E) = -\frac{1}{\pi} P \int_{-\infty}^{\infty} \frac{1}{E - E'} \mathrm{Im}G(E')\mathrm{d}E' \,. \tag{62}$$

Another useful relation for the Green function is given by

$$\frac{\mathrm{d}G(E)}{\mathrm{d}E} = \frac{\mathrm{d}}{\mathrm{d}E}\frac{1}{E - \mathcal{H}} = -\frac{1}{E - \mathcal{H}}\frac{1}{E - \mathcal{H}} = -G(E)G(E) \,, \tag{63}$$

which leads to

$$G_{00}(E_F) = \int^{E_F} \frac{\mathrm{d}G_{00}(E)}{\mathrm{d}E}\mathrm{d}E = -\int^{E_F} \sum_i G_{0i}(E)G_{i0}(E)\mathrm{d}E \,, \tag{64}$$

where explicitly the position dependence was denoted. The Green functions for the potentials $V^{\pm}(\underline{r}) = V^o(\underline{r}) + \Delta V^{\pm}(\underline{r})$ are connected with the Green function for the non-magnetic state with potential $V^o(\underline{r})$ by the Dyson equation

$$G^{\pm} = G^o + G^o \Delta V^{\pm} G^{\pm} \,, \tag{65}$$

which follows from the fact that the inverse operators $(G^o)^{-1}$, $(G^{\pm})^{-1}$ can be written as

$$(G^o)^{-1} = E - \mathcal{H}^o \,, \qquad (G^{\pm})^{-1} = E - \mathcal{H}^{\pm} \,. \tag{66}$$

where the Hamilton operators according to $\mathcal{H}^{\pm} = \mathcal{H}^{o} + \Delta V^{\pm}$ differ by $\Delta V^{\pm} = V^{\pm} - V^{o}$. This leads to $(G^{\pm})^{-1} = (G^{o})^{-1} - \Delta V^{\pm}$, which solved for $G^{\pm}$ gives equation (65). For small potential differences the expansion of Eq. (65) is given by

$$G^{+} - G^{-} = G^{o}(\Delta V^{+} - \Delta V^{-})G^{o} + \dots . \tag{67}$$

References

1. U. von Barth and L. Hedin, *A local exchange-correlation potential for the spin polarized case: I*, J. Phys. C **5**, 1629–1642 (1972).
2. M. M. Pant and A. K. Rajagopal, *Theory of inhomogeneous magnetic electron gas*, Solid State Commun. **10**, 1157–1160 (1972).
3. H. Eschrig, M. Sargolzaei, K. Koepernik, and M. Richter, *Orbital polarization in the Kohn-Sham-Dirac theory*, Europhys. Lett. **72**, 611–617 (2005).
4. S. H. Vosko, L. Wilk, and M. Nusair, *Accurate spin-dependent electron liquid correlation energies for local spin density calculations: a critical analysis*, Can. J. Phys. **58**, 1200–1211 (1980).
5. J. P. Perdew and A. Zunger, *Self-interaction correction to density-functional approximations for many-electron systems*, Phys. Rev. B **23**, 5048–5079 (1981).
6. J. P. Perdew, J. A. Chevary, S. H. Vosko, K. A. Jackson, M. R. Pederson, D. J. Singh, and C. Fiolhais, *Atoms, molecules, solids, and surfaces: Applications of the generalized gradient approximation for exchange and correlation*, Phys. Rev. B **46**, 6671–6687 (1992); Phys. Rev. B **48**, 4978 (1993).
7. J. P. Perdew, K. Burke, and M. Ernzerhof, *Generalized Gradient Approximation Made Simple*, Phys. Rev. Lett. **77**, 3865–3868 (1996).
8. S. H. Vosko, J. P. Perdew, and A. H. MacDonald, *Ab Initio Calculation of the Spin Susceptibility for the Alkali Metals Using the Density-Functional Formalism*, Phys. Rev. Lett. **35**, 1725–1728 (1975).
9. U. K. Poulsen, J. Kollar, and O. K. Andersen, *Magnetic and cohesive properties from canonical bands*, J. Phys. F **6**, L241–L247 (1976).
10. O. Gunnarsson, *Band model for magnetism of transition metals in the spin-density-functional formalism*, J. Phys. F **6**, 587–606 (1976).
11. O. Gunnarsson, *Band magnetism in the spin-density-functional formalism*, J. Appl. Phys. **49**, 1399–1404 (1978).
12. E. C. Stoner, *Collective Electron Specific Heat and Spin Paramagnetism in Metals*, Proc. Roy. Soc. A **154**, 656-678 (1936).
13. E. C. Stoner, *Collective Electron Ferromagnetism*, Proc. Roy. Soc. A **165**, 372–414 (1938).
14. E. C. Stoner, *Collective Electron Ferromagnetism II: Energy and Specific Heat*, Proc. Roy. Soc. A **169**, 339–371 (1939).
15. J. F. Janak, *Uniform susceptibilities of metallic elements*, Phys. Rev. B **16**, 255–262 (1977).
16. J. F. Janak, *Itinerant ferromagnetism in fcc cobalt*, Solid State Commun. **25**, 53–55 (1978).
17. V. L. Moruzzi, J. F. Janak, and A. R. Williams, *Calculated Electronic Properties of Metals* (Pergamon Press, New York, 1978).

18. A. P. Malozemoff, A. R. Williams, and V L. Moruzzi, *"Band gap theory" of strong ferromagnetism: Application to concentrated crystalline and amorphous Fe- and Co-metalloid alloys*, Phys. Rev. B **29**, 1620–1631 (1984).
19. P. H. Dederichs and R. Zeller, *Self-consistency iterations in electronic-structure calculations*, Phys. Rev. B **28**, 5462–5472 (1983).
20. D. G. Anderson, *Iterative Procedures for Nonlinear Integral Equations*, J. Assoc. Comput. Mach. **12**, 547–560 (1965).
21. C. G. Broyden, *A Class of Methods for Solving Nonlinear Simultaneous Equations*, Math. Comput. **19**, 577–593 (1965).
22. S. Blügel, Ph.D. thesis, *First Principles Calculations of the Electronic Structure of Magnetic Overlayers on Transition Metal Surfaces* (Rheinisch-Westfälische Technische Hochschule Aachen), Berichte der Kernforschungsanlage Jülich Nr. 2197 (1987).
23. V. Eyert, *A Comparative Study on Methods for Convergence Acceleration of Iterative Vector Sequences*, J. Comp. Phys. **124**, 271–285 (1996).
24. M. A. Van Hove and G. A. Somorjai, *A new microfacet notation for high-Miller-index surfaces of cubic materials with terrace, step and kink structures*, Surf. Sci. **92**, 489-518 (1980).
25. T. Asada, G. Bihlmayer, S. Handschuh, S. Heinze, Ph. Kurz, and S. Blügel, *First-principles theory of ultrathin magnetic films*, J. Phys.: Condensed Matter **11**, 9347–9363 (1999).
26. M. Donath, *Magnetic order and electronic structure in thin films*, J. Phys.: Condensed Matter **11**, 9421–9436 (1999).
27. P. Poulopoulos and K. Baberschke, *Magnetism in thin films*, J. Phys.: Condensed Matter **11**, 9495–9515 (1999).
28. M. Weinert and A. J. Freeman, *Magnetism of linear chains*, J. Magn. Magn. Mater. **38**, 23–33 (1983).
29. N. Zabala, M. J. Puska, and R. M. Nieminen, *Spontaneous Magnetization of Simple Metal Nanowires*, Phys. Rev. Lett. **80**, 3336-3339 (1998); Phys. Rev. Lett. **82**, 3000 (1999).
30. O. A. Starykh and D. L. Maslov, *Comment on "Spontaneous Magnetization of Simple Metal Nanowires"*, Phys. Rev. Lett. **82**, 2999 (1999).
31. D. I. Bazhanov, W. Hergert, V. S. Stepanyuk, A. A. Katsnelson, P. Rennert, K. Kokko, and C. Demangeat, *One-dimensional magnetism of Rh chains on the Ag(001) surface*, Phys. Rev. B **62**, 6415–6420 (2000).
32. S. Okada and A. Oshiyama, *Magnetic ordering of Ga wires on Si(100) surfaces*, Phys. Rev. B **62**, R13286–R13289 (2000).
33. V. Bellini, N. Papanikolaou, R. Zeller, and P. H Dederichs, *Magnetic $4d$ monoatomic rows on Ag vicinal surfaces*, Phys. Rev. B **64**, 094403 (2001).
34. M. Eisenbach, B. L. Gyorffy, G. M. Stocks, and B. Ujfalussy, *Magnetic anisotropy of monoatomic iron chains embedded in copper*, Phys. Rev. B **65**, 144424 (2002).
35. D. Spisak and J. Hafner, *Fe nanowires on vicinal Cu surfaces: Ab initio study*, Phys. Rev. B **65**, 235405 (2002).
36. A. Ayuela, H. Raebiger, M. J. Puska, and R. M. Nieminen, *Spontaneous magnetization of aluminum nanowires deposited on the NaCl(100) surface*, Phys. Rev. B **66**, 035417 (2002).
37. M. Komelj, C. Ederer, J. W. Davenport, and M. Fähnle, *From the bulk to monatomic*

wires: An ab initio study of magnetism in Co systems with various dimensionality, Phys. Rev. B **66**, 140407 (2002).
38. D. Spisak and J. Hafner, *Magnetism of monoatomic wires on vicinal surfaces*, Comput. Mater. Sci. **27**, 138–150 (2003).
39. D. Spisak and J. Hafner, *Magnetism of ultrathin wires suspended in free space and absorbed on vicinal surfaces*, Phys. Rev. B **67**, 214416 (2003).
40. J. Hong and R. Q. Wu, *First principles calculations of magnetic anisotropy energy of Co monatomic wires*, Phys. Rev. B **67**, 020406 (2003).
41. A. Bergara, J. B. Neaton, and N. W. Ashcroft, *Ferromagnetic Instabilities in Atomically Thin Lithium and Sodium Wires*, Int. J. Quantum Chem. **91**, 239–244 (2003).
42. A. Delin and E. Tosatti, *Magnetic phenomena in 5d transition metal nanowires*, Phys. Rev. B **68**, 144434 (2003).
43. A. Delin and E. Tosatti, *Emerging magnetism in platinum nanowires*, Surf. Sci. **566–568**, 262–267 (2004).
44. A. Delin, E. Tosatti, and R. Weht, *Magnetism in Atomic-Size Palladium Contacts and Nanowires*, Phys. Rev. Lett. **92**, 057201 (2004).
45. A. Delin and E. Tosatti, *The electronic structure of 4d transition-metal monatomic wires*, J. Phys.: Condensed Matter **16**, 8061–8074 (2004).
46. M. M. Rahman, M. Kisaku, T. Kishi, D. Matsunaka, W. A. Dino, H. Nakanishi, and H. Kasai, *Ab initio study of magnetic and electronic properties of Fe-filled single-walled carbon nanotubes*, J. Phys.: Condensed Matter **16**, S5755–S5758 (2004).
47. B. Lazarovits, B. Ujfalussy, L. Szunyogh, G. M. Stocks, and P. Weinberger, *Ab initio study of canted magnetism of finite atomic chains at surfaces*, J. Phys.: Condensed Matter **16**, S5833–S5840 (2004).
48. T. J. Yang, Y.-J. Zhao, and A. J. Freeman, *Magnetism and electronic structure of Fe chains and nano-wires*, J. Magn. Magn. Mater. **272–276**, 1648–1649 (2004).
49. C. Jo and J. I. Lee, *Structures and magnetic properties of Fe_n (n=1-4) nanowires*, Phys. Status Solidi b **241**, 1427–1430 (2004).
50. Y. Mokrousov, G. Bihlmayer, and S. Blügel, *Full-potential linearized augmented plane-wave method for one-dimensional systems: Gold nanowire and iron monowires in a gold tube*, Phys. Rev. B **72**, 045402 (2005).
51. R. Zeller, P. H. Dederichs, B. Ujfalussy, L. Szunyogh, and P. Weinberger, *Theory and convergence properties of the screened Korringa-Kohn-Rostoker method*, Phys. Rev. B **52**, 8807–8812 (1995).
52. R. Zeller, *Evaluation of the screened Korringa-Kohn-Rostoker method for accurate and large-scale electronic-structure calculations*, Phys. Rev. B **55**, 9400–9408 (1997).
53. K. Wildberger, R. Zeller, and P. H. Dederichs, *Screened KKR-Green's-function method for layered systems*, Phys. Rev. B **55**, 10074–10080 (1997).
54. N. Papanikolaou, R. Zeller, and P. H. Dederichs, *Conceptual improvements of the KKR method*, J. Phys.: Condensed Matter **16**, 2799–2823 (2002).
55. K. Wildberger, V. S. Stepanyuk, P. Lang, R. Zeller, and P. H. Dederichs, *Magnetic Nanostructures: 4d Clusters on Ag(001)*, Phys. Rev. Lett. **75**, 509-512 (1995).
56. G. Kresse and J. Furthmüller, *Efficient iterative schemes for ab initio total-energy calculations using a plane-wave basis set*, Phys. Rev. B **54**, 11169-11186 (1996).
57. G. Kresse and J. Furthmüller, *Efficiency of ab-initio total energy calculations for met-*

als and semiconductors using a plane-wave basis set, Comput. Mater. Sci. **6**, 15–50 (1996).
58. J. Deutz, P. H Dederichs, and R. Zeller, *Local density of states of impurities in Al*, J. Phys. F **11**, 1787–1800 (1981).
59. S. Blügel, *Ferromagnetism of 4d-metal monolayers on Ag, Au and Pd(001) surfaces*, Europhys. Lett. **18**, 257–262 (1992).
60. A. R. Williams, R. Zeller, V. L. Moruzzi, C. D. Gelatt, Jr., and J. Kübler, *Covalent magnetism: An alternative to the Stoner model*, J. Appl. Phys. **52**, 2067–2069 (1981).
61. A. Oswald, R. Zeller, P. J. Braspenning, and P. H Dederichs, *Interaction of magnetic impurities in Cu and Ag*, J. Phys. F **15**, 193–212 (1985).
62. M. Asato, A. Settels, T. Hoshino, T. Asada, S. Blügel, R. Zeller, and P. H. Dederichs, *Full-potential KKR calculations for metals and semiconductors*, Phys. Rev. B **60**, 5202-5210 (1999).
63. R. Hafner, D. Spisak, R. Lorenz, and J. Hafner, *Magnetic ground state of Cr in density-functional theory*, Phys. Rev. B **65**, 184432 (2002).
64. S. Cottenier, B. De Vries, J. Meersschaut, and M. Rots, *What density-functional theory can tell us about the spin-density wave in Cr*, J. Phys.: Condensed Matter **14**, 3275–3283 (2002).